Optical properties of pyrolytic boron nitride in the energy range 0.05—10 eV

D. M. Hoffman, G. L. Doll, and P. C. Eklund
Department of Physics and Astronomy, University of Kentucky, Lexington, Kentucky 40506
(Received 15 June 1984)

Optical reflectance studies of the c face of pyrolytic boron nitride were carried out at room temperature in the photon energy range 0.045—10 eV. A Kramers-Kronig analysis was performed to determine the in-plane real (ϵ_1) and imaginary (ϵ_2) dielectric functions. Infrared-active transverse-optic phonons were observed at 770 and 1383 cm^{-1}. Strong impurity- and defect-associated absorption was observed throughout the visible and near-ultraviolet region (1—5 eV) which masks, to some extent, the threshold for absorption across the electronic energy band gap. From $\epsilon_2(\omega)$ and the absorption coefficient we estimate the direct band gap between π bands to be 5.2±0.2 eV. Interband transitions associated with high joint density of states were observed at 6.10 and 6.85 eV. The structure in $\epsilon_2(\omega)$ at energies $\hbar\omega > 5$ eV is identified with specific transitions predicted by previous energy-band calculations.

I. INTRODUCTION

Hexagonal pyrolytic boron nitride has in recent years become a material of considerable technological importance to the GaAs semiconductor industry and material science as a new crucible material used for purifying and preparing new compounds. From a fundamental scientific viewpoint, boron nitride (BN) represents an interesting quasi-two-dimensional, insulating analog to semimetallic graphite. Both BN and graphite share the same point group (D_{6h}) and have a crystal structure in which atoms are arranged hexagonally into layers having strong intralayer bonds and weak interlayer bonds.

Whereas the agreement between electronic energy-band calculations and experiment is now considered quite good for the case of graphite,[1–4] there still exists considerable disagreement between experiment and theory in this area in BN. For example, values for the band gap in BN span a rather wide range: 3.2—5.8 eV (experimental)[5–13] and 2.45—12.7 eV (calculated).[8,10,14–20] Electronic absorption has been studied in the ultraviolet by photoluminescence,[5] electron-energy-loss spectroscopy (EELS),[6,7] transmission,[8–10] ellipsometry,[11] and x-ray emission.[12,13] To our knowledge no single optical study has been carried out over a photon energy range of sufficient width to allow an accurate determination (via Kramers-Kronig relations) of the optical constants.

In this paper we present the results of such a study. We have measured the reflectance at near-normal incidence of well-characterized samples of pyrolytic boron nitride in the photon energy range 0.045—10 eV and determined the dielectric function $\epsilon(\omega)=\epsilon_1(\omega)+i\epsilon_2(\omega)$ and the electron-energy-loss function $\mathrm{Im}(-1/\epsilon)$. These experimental results will be compared to reported electron-energy-band calculations.[8,10,14–17]

II. EXPERIMENTAL DETAILS AND SAMPLE CHARACTERIZATION

A large plate ($6\times10\times0.1$ cm^3) of pyrolytic boron nitride (p-BN) prepared by high-temperature chemical vapor deposition (CVD) onto a graphite substrate was obtained from Union Carbide.[21] Smaller samples used for the spectroscopic measurements ($8\times8\times1$ mm^3) were cut from the original plate using a diamond wire saw and subsequently polished to an optical finish with a succession of finer particle-size grits. The final polish was accomplished with 0.05 μm alumina powder (Buehler) and distilled water. The samples were then washed in spectral grade carbon tetrachloride.

The structure of hexagonal boron nitride, as determined by Pease,[22] is shown in Fig. 1. Strong sp^2 bonds between boron and nitrogen atoms result in the hexagonal organization shown, where the boron atoms are threefold coordinated to nitrogen atoms. Hexagonal BN exhibits $ABAB\ldots$ stacking[22] with boron atoms in layer A found directly below nitrogen atoms in layer B. The $ABAB\ldots$ stacking in graphite is associated with a glide displacement between adjacent carbon layers such that the corners of the hexagons in one layer are directly above (or below)

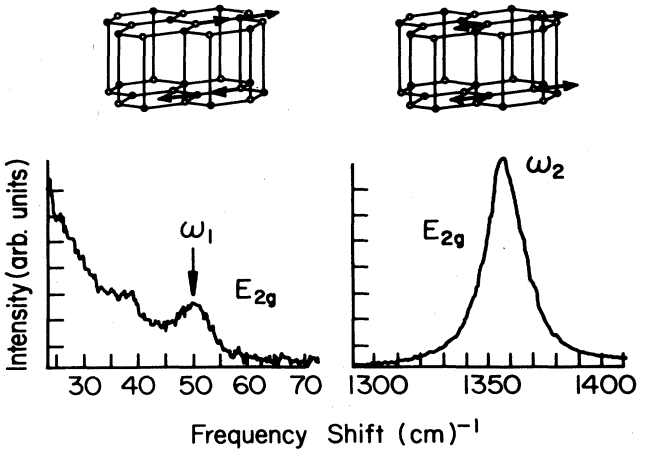

FIG. 1. Raman spectra and normal modes of E_{2g} intralayer modes. The data were taken on the c face in the Brewster-angle backscattering geometry.

the centers of hexagons in the next layer. X-ray (00l) diffraction scans of our p-BN samples were obtained using a GE XRD-6 diffractometer equipped with a Mo x-ray source and an energy-dispersive Si:Li detector. The interplane spacing along the c axis determined from the peak positions was found to be $\frac{1}{2}c=3.33$ Å. This value agrees with that reported by Pease[22] for well-annealed p-BN samples, compares well with that of single-crystal BN (3.315 Å),[23] and is within the range of $\frac{1}{2}c=3.33$–3.43 Å (Ref. 24) previously reported for CVD pyrolytic BN. This range of c-axis values for CVD p-BN may be responsible for the poor agreement between various experimental values for the energy band gap. We observe a full width at half maximum (FWHM) for the (001) reflection of 1.02°. This indicates that although our pyrolytic boron nitride samples were polycrystalline in the basal plane, there is long-range c-axis stacking order (~ 70 Å) and good c-axis alignment among the crystallites over several mm^2 area (x-ray beam diameter ≈ 2 mm).

To further characterize our samples we measured the Raman spectrum in the range of first-order scattering (0–1400 cm^{-1}). The Raman spectrum (~ 300 K) of p-BN is shown in Fig. 1. The spectrum was taken in the Brewster angle backscattering geometry with the Raman-scattered radiation collected along the c axis of the sample. Radiation (4880 Å) from a Spectra Physics 164 argon-ion laser was used to excite the modes. A Spex 1402 double-holographic grating monochromator and a dry-ice-cooled ITT FW130 photomultiplier tube interfaced to a microcomputer were used to acquire the spectrum.

Two Raman-active (E_{2g}) modes[25–31] were observed at 49 and 1367 cm^{-1}, with respective full width at half-maximum intensity of ~ 3 and ~ 16 cm^{-1}. We believe the weaker feature at 38 cm^{-1} to be an artifact and not attributable to the sample. The widths are corrected for the monochromator resolution (~ 4 cm^{-1}). The nature of these zone-center normal modes ($q=0$ phonons) is shown as insets in Fig. 1. The frequencies we report (49 and 1367 cm^{-1}) are in good agreement with those reported by other workers.[9,25–29] The FWHM of the 1367-cm^{-1} mode is twice that measured by Kuzuba *et al.*[29] for single crystals, but only $\sim\frac{1}{4}$ that measured by Geick *et al.*[25] for p-BN. The position and FWHM of the 1367-cm^{-1} mode have been shown[27,28] to vary linearly with inverse crystallite size (basal-plane dimension). The peak position down shifts by ~ 8 cm^{-1} and the FWHM decreases from 40 to 9 cm^{-1} as the basal-plane crystallite size varies from 35 to 500 Å. This suggests that the crystallites in our CVD p-BN samples have an average basal-plane diameter of ~ 190 Å.

The reflectance of p-BN was studied over the photon energy range 0.045–10 eV (with light at near-normal incidence to the polished c face). A $\frac{1}{4}$-m grating monochromator (Spex model no. 1670) with globar and W-filament sources, six gratings, order sorting filters, and a pyroelectric detector were used in the infrared and visible regions. This spectrometer covered the range from 0.045–2.0 eV. A prism monochromator (Perkin-Elmer model no. 83) with a quartz prism, W-filament and deuterium lamp sources, MgF_2-coated aluminum mirror optics, and a photomultiplier detector were used in the visible-uv spectral region from 1.5 to 6.2 eV. In each of these spectrometers the sample reflectance was determined using single-beam optics by substituting a standard mirror for the sample at each wavelength. Sample and standard mirror were mounted adjacent to one another on a optical translation table whose position is computer controlled. The reflectance is thus the ratio of the intensities reflected from the sample and standard mirror corrected for the reflectance of the standard mirror. Evaporated Au films were used as the standard in the infrared while a MgF_2-coated aluminum film was used for the visible and ultraviolet regions. The absolute reflectance of p-BN was measured for photon energies from 5.0 to 10.0 eV using a McPherson model no. 225 (Seya-Namioka) monochromator with a Hintenrigger H_2 lamp. A rotatable sodium salicylate-coated light pipe and external photomultiplier tube were used as the detector. The sample chamber was evacuated to $\sim 10^{-6}$ Torr.

III. RESULTS AND DISCUSSION

Reflectance data from the three spectrometers discussed in Sec. II were joined together to form the spectrum $R(\omega)$, $0.045<\hbar\omega<10$ eV shown in Fig. 2. Low- and high-energy extensions of the data were added in order to carry out the Kramers-Kronig transformation of $R(\omega)$ to yield the dielectric function

$$\epsilon(0,\omega)=\epsilon_1(0,\omega)+i\epsilon_2(0,\omega)\equiv\epsilon_1(\omega)+i\epsilon_2(\omega)\ .$$

Since BN is an insulator, the reflectance data were extrapolated below 0.045 eV as a constant. The high-energy extension of $R(\omega)$ was carried out using (1) the data of Mamy *et al.*[11] (10–30 eV), (2) $R(\omega)\sim\omega^{-10}$ (30–100 eV), and (3) thereafter as $R(\omega)\sim\omega^{-4}$.

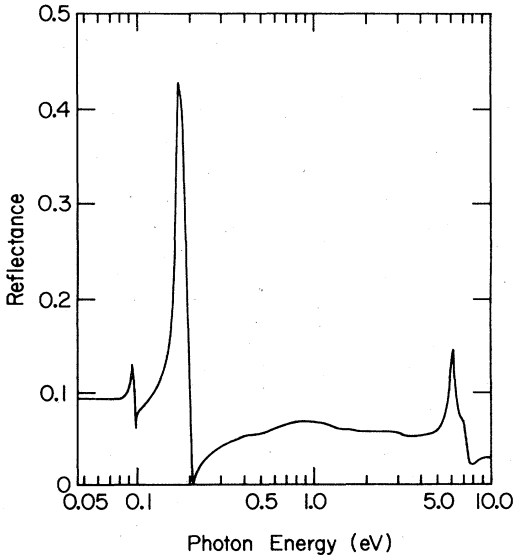

FIG. 2. Reflectance of pyrolytic boron nitride taken at near-normal incidence to the c face at 300 K.

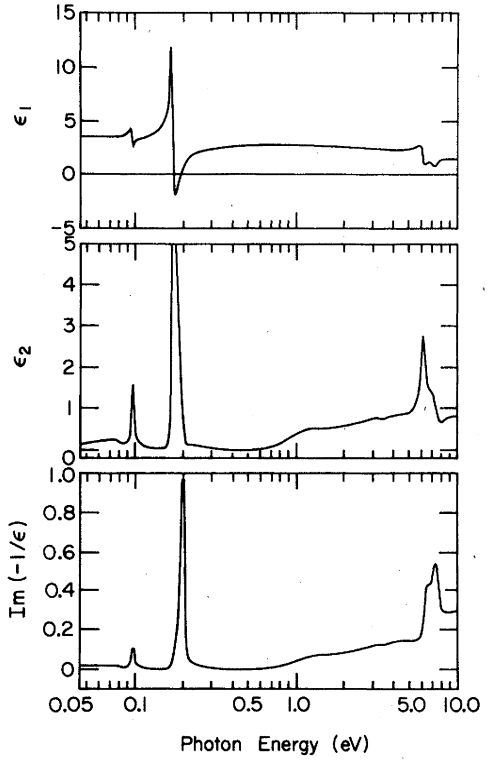

FIG. 3. Real and imaginary dielectric constants and electron-energy-loss function of pyrolytic boron nitride determined by a Kramers-Kronig analysis of the data displayed in Fig. 2.

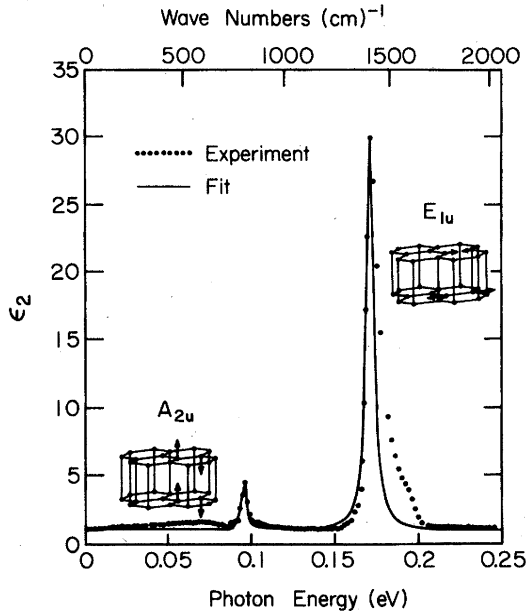

FIG. 4. Imaginary dielectric constant, $\epsilon_2(\omega)$, in the infrared region. The structure is due to transverse-optic phonons with frequencies of 770 and 1383 cm^{-1}. The data were fitted to Lorentzian line shapes (Table I) represented by the solid line. The misfit on the high-energy side of the E_{1u} phonon is identified with two-phonon absorption.

The data (and extensions) were transformed according to standard techniques[32] to yield the real (ϵ_1) and imaginary parts (ϵ_2) of the dielectric function. The process involves the calculation of the phase-shift integral $\theta(\omega)$,

$$\theta(\omega_0)=\frac{\omega_0}{\pi}\int_0^\infty \frac{\ln[R(\omega)/R(\omega_0)]}{\omega_0^2-\omega^2}d\omega\ . \tag{1}$$

Once the phase-shift integral $\theta(\omega)$ is known, $\epsilon_1(\omega)$ and $\epsilon_2(\omega)$ can be calculated directly without approximation.[33] In Fig. 3 we display the results of the Kramers-Kronig transformation. The functions $\epsilon_1(\omega)$, $\epsilon_2(\omega)$, and $\mathrm{Im}[-1/\epsilon(\omega)]$ are displayed on a logarithmic photon energy scale.

Turning our attention to the upper panel $[\epsilon_1(\omega)]$, features at $\sim$0.1 and $\sim$0.2 eV are associated with transverse-optic (TO) photons. Below $\sim$0.07 eV $\epsilon_1(\omega)$ is seen to be constant and has the value $\epsilon_1=3.55$. This value is to be compared with the value 5.12 obtained at 4 GHz using microwave techniques on similar material.[24]

Low-energy features in $\epsilon_2(\omega)$ (middle panel of Fig. 3) corresponding to the TO phonons appear as sharp lines at $\sim$0.1 and $\sim$0.2 eV. This frequency region has been replotted in Fig. 4 where the dots represent the data and the solid line represents the results of a Lorentz oscillator fit to the TO-phonon features. The symmetry labels in the figure are in agreement with assignments made in previous work.[25,31] Also shown are schematic views of the respective ir-active, in-plane (high-frequency), and out-of-plane (low-frequency) modes associated with the E_{1u} and A_{2u} zero wave-vector phonons. The TO-phonon data were analyzed in the usual manner by fitting the infrared region to the expression[34]

$$\epsilon(\omega)=\epsilon_\infty+\sum_j \frac{f_j}{\omega_j^2-\omega^2-i\omega\Gamma_j}\ , \tag{2}$$

where ϵ_∞ is the high-frequency dielectric constant and f_j, Γ_j, ω_j are the oscillator strength, half-width and frequency of the jth phonon. A comparison of our results with that of Geick *et al.*[25] can be found in Table I. Of particu-

TABLE I. Infrared TO phonon in *p*-BN. The parameters (ω_j, Γ_j, f_j) were determined by a Lorentz oscillator fit to $\epsilon_2(\omega)$, see Eq. (2) in the text.

	A_{2u} (out of plane)			E_{1u} (in plane)		
	ω_1 (cm^{-1})	Γ_1 (cm^{-1})	$10^4 f_1$ (cm^{-2})	ω_2 (cm^{-1})	Γ_2 (cm^{-1})	$10^6 f_2$ (cm^{-2})
This work	770±3	18[a]±4	3.8±0.1	1383±5	30[a]±4	0.75±0.01
Geick *et al.* (Ref. 25)	767	35	12.3	1367	29	3.49

[a]Corrected for instrument resolution.

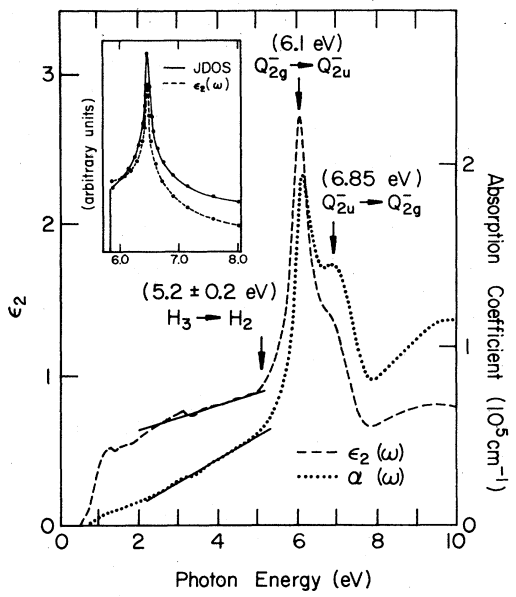

FIG. 5. Imaginary dielectric constant, $\epsilon_2(\omega)$, and absorption coefficient, $\alpha(\omega)$, due to electronic absorption in pyrolytic boron nitride. The absorption below ~5 eV is identified with impurity and/or defect states. The threshold for $\pi \rightarrow \pi$ band absorption is indicated at 5.2 eV. The transition assignment labels in the figure are consistent with those found in the right-hand panel of Fig. 6.

lar significance is that the TO frequencies found in this work are somewhat higher, especially in the case of the in-plane (E_{1u}) phonon. This may well be due to differences in the samples. The three samples we measured, which came from the same large p-BN plate, yielded values within the error listed in Table I. On the high-energy side of the E_{1u} phonon the deviation of the data from the Lorentzian line shape shown (Fig. 4) is due to the presence of additional two-phonon absorption. The A_{1u} out-of-plane mode cannot be excited at normal incidence ($\vec{E} \perp \vec{c}$), however, at near-normal incidence some incident rays have an $\vec{E} \| \vec{c}$ component which does couple to the A_{1u} mode. The oscillator strength (Table I) for this mode is therefore of little quantitative value.

Electronic absorption begins at ~1 eV, as can be seen in the middle and lower panels of Fig. 3. A broad continuum is observed from ~1 to ~5 eV; above 5 eV the absorption rises abruptly due to intrinsic interband transitions ($\pi \rightarrow \pi$) across the insulating band gap. We attribute the 1—5 eV continuum to transitions involving impurity and defect states distributed throughout the gap. This impurity absorption is strong and also broadens the onset of $\pi \rightarrow \pi$ transition. In Fig. 5 we display $\epsilon_2(\omega)$ and the absorption coefficient $\alpha(\omega)$ on a linear energy scale to display clearly the separation of the impurity absorption and the $\pi \rightarrow \pi$ threshold. The inset in the figure is due to calculations by Doni and Parravicini[14] based on a two-dimensional, tight-binding calculation and indicates the joint density-of-states (JDOS) function and $\epsilon_2(\omega)$ for the onset of $\pi \rightarrow \pi$ transitions. The curves in the inset to Fig. 5 show a steep rise near ~5.8 eV followed by a single peak near ~6.6 eV, in qualitative agreement with the data. The data, however, show a peak at 6.10 eV *and a shoulder at 6.85 eV.* The shoulder at 6.85 eV is associated with c-axis dispersion, a point which we discuss later.

Several other band calculations have also been reported. The direct band gaps associated with these energy-band calculations are as follows: Taylor and Coulson,[18] 4.6 eV (2D); Nakhmanson and Smirnov,[15] 2.45 eV (3D); Zupan and Kolar,[8] 4.9 eV (3D); Zunger *et al.*,[10] 3.7, 5.1, and 5.5 eV (2D); Zunger,[19] 2.95 and 5.44 eV (2D); Dovesi *et al.*,[20] 12.7 eV (2D); Robertson,[17] 4.2 eV (3D). The abbreviations 2D and 3D refer to two- and three-dimensional band cal-

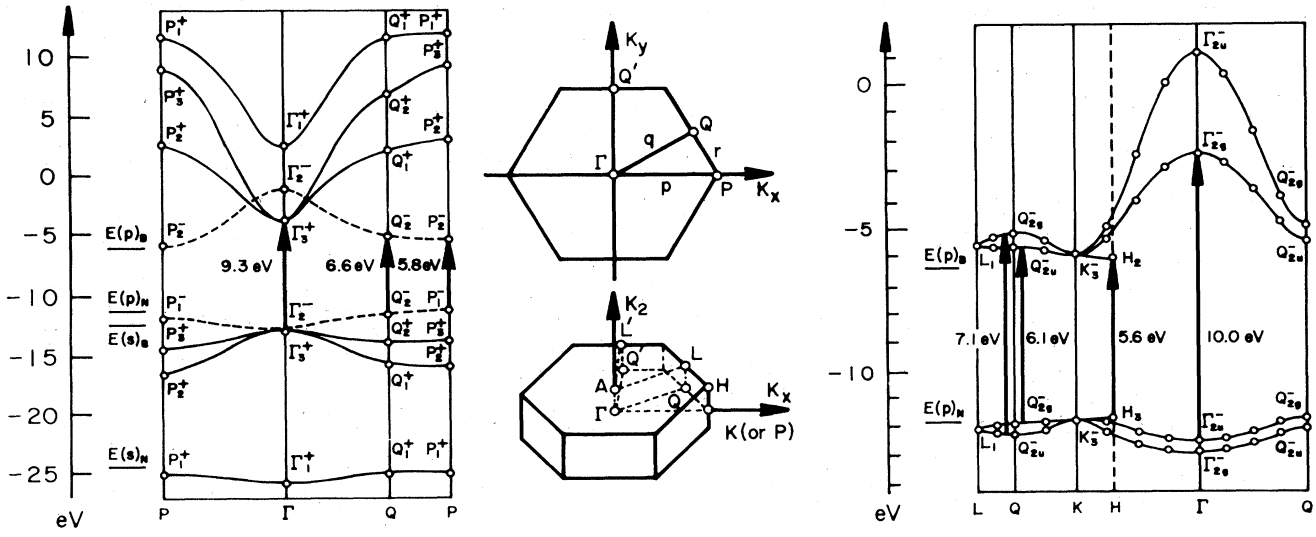

FIG. 6. Two- and three-dimensional band structures and corresponding Brillouin zones of hexagonal boron nitride. The calculations are due to Doni and Parravicini, Ref. 14.

TABLE II. Low-energy optical transitions allowed for $\vec{E}\perp\vec{c}$ which contribute to $\epsilon_2(\omega)$. All transition energies are in eV. The symmetry labels are consistent with those found in Figs. 5 and 6. OPW denotes orthogonalized plane wave calculation. EXH, SIEXH, and MIEXH denote extended, simplified iterative, and modified iterative Hückel calculations, respectively.

	$H_3\rightarrow H_2$ (Band gap)	$Q_{2g}^-\rightarrow Q_{2u}^-$		$Q_{2u}^-\rightarrow Q_{2g}^-$
Experiment				
This work	5.2	6.10		6.85
Reflectance				
Cazaux (Ref. 6)			6.3[a]	
EELS				
Vilanove (Ref. 7)	<5.0		6.5[a]	
EELS				
Mamy *et al.* (Ref. 11)		6.0		6.7
Ellipsometry				
Choyke in Ref. 14	5.6	6.2		7.0
Reflectance				
3D Band structures				
Doni and Parravicini (Ref. 14)	5.6	6.1		7.1
Tight binding				
Nakhmanson and Smirnov (Ref. 15)	2.45	3.2		5.2
OPW				
Zupan *et al.* (Refs. 8 and 16)	4.9	6.4		11.0
Tight binding				
Robertson (Ref. 17)	4.2	6.5		7.9
Tight binding				
	$P_1^-\rightarrow P_2^-$ (Band gap)		$Q_2^-\rightarrow Q_2^-$	
2D Band structures				
Doni and Parravicini (Ref. 14)	5.8		6.7	
Tight binding				
Zunger *et al.* (Ref. 10)				
EXH	5.5		6.3	
SIEXH	3.7		6.0	
MIEXH	5.1		6.3	

[a]No high-energy shoulder evident near ~ 7 eV.

culations. These values would suggest that pure and defect-free BN should be transparent in the visible and near-ultraviolet range. The white color of *p*-BN is therefore not intrinsic but associated with impurity and defect states in the band gap. The wide range of experimental values reported for the band gap may in large part be due to the presence of these gap states: Larach and Shrader[5] (photoluminescence), 5.5. eV; Zupan and Kolar[8] (absorption), 4.3 eV; Baronian[9] (absorption), 5.8 eV; Zunger *et al.*[10] (absorption), 5.8 eV; Fomichev[12] (x-ray emission), 3.6 eV; Tegeler *et al.*[13] (x-ray emission), 3.2 eV.

These values for the band gap are to be compared to a value of 5.2 ± 0.2 determined from this work. We identify the band gap by the position in energy of the rapid change in slope (Fig. 5) of $\epsilon_2(\omega)$ or $\alpha(\omega)$ which occurs as the contribution from the $\pi\rightarrow\pi$ transitions to the total absorption becomes evident relative to the impurity background absorption. The thick solid lines in the figure represent an extrapolated background and serve as a guide to the eye.

In Fig. 6 we show representative 2D and 3D tight-binding energy-band calculations[14] for BN in the left- and right-hand panels, respectively. The 2D and 3D hexagonal Brillouin zones are shown between these panels. Important low-energy optical transitions ($q=0$), allowed in near-normal incidence experiments on the *c* face ($\vec{E}\perp\vec{c}$), are indicated as bold vertical arrows in the panels. The corresponding photon energies $\hbar\omega=E_f-E_i$, where E_i and E_f refer to the initial and final electronic energies, are also indicated next to the respective arrow in the figure. When they were not tabulated,[14,15,17] we have estimated values for these optical energies from the dispersion curves.

From Fig. 6 we see that the direct energy gap is associated with the *P* point ($P_1^-\rightarrow P_2^-$) and with the *H* point ($H_3\rightarrow H_2$) in the 2D and 3D calculations, respectively. Although all reported calculations exhibit bands of similar form to those of Doni and Parravicini[14] displayed in the figure, the results of these authors compare most favorably with structure in our data in the 5—10 eV region. We compare other experimental and theoretical results for structure in this energy region in Table II. Experimental results appear first, followed by results of 3D and 2D calculations.

Returning to the energy bands displayed in the left- and right-hand panels of Fig. 6, we see that the bands found in the right-hand panel (3D) are associated only with the bands indicated by dashed lines in the left-hand panel (2D). (The two panels are plotted with different energy scales.) 3D calculations[8,14–17] show that the gap occurs at the H point, rather than the K point, because of c-axis dispersion. The interlayer interaction in BN is also seen to produce significant splitting in the π bands, as is evident in the figure. This splitting gives rise to two transitions ($Q_{2g}^- \rightarrow Q_{2u}^-$ and $Q_{2u}^- \rightarrow Q_{2g}^-$) at the Q point, rather than the one transition ($Q_2^- \rightarrow Q_2^-$) predicted in 2D calculations. Thus, the 3D JDOS function would appear similar to that shown in the inset of Fig. 5, but would have an additional high-energy shoulder, such as the one that appears at 6.85 eV in our experimental $\epsilon_2(\omega)$. The symmetry labels indicated in Fig. 5 are consistent with those found in the right-hand panel of Fig. 6. We identify the peaks in $\epsilon_2(\omega)$ at 6.10 and 6.85 eV with the Q point in the 3D calculations. Assuming this assignment is correct, these peaks provide a direct measure of the c-axis dispersion. This point was also appreciated by Doni and Parravicini[14] in reference to peaks in $\epsilon_2(\omega)$ at 6.2 and 7.0 eV in the unpublished data of Choyke. As far as we know, the data of Choyke have never been published. Peaks in $\epsilon_2(\omega)$ at 6.0 and 6.7 eV determined by ellipsometry[11] have been reported recently and are in good agreement with the unpublished results of Choyke[14] and this work.

IV. SUMMARY AND CONCLUSIONS

We have studied the optical reflectance ($\vec{E} \perp \vec{c}$) of chemically vapor-deposited pyrolytic boron nitride in the energy range 0.045–10 eV. We find a value of 3.55 for the static dielectric constant, and TO phonons were observed at 770 and 1383 cm^{-1}. In the region 1–5 eV, strong impurity- and/or defect-associated absorption was observed which masks and broadens the onset of $\pi \rightarrow \pi$ transitions at 5.2 eV. Further structure in $\epsilon_2(\omega)$ is found at 6.10 and 6.85 eV which is attributed to π-band splitting at the Q point consistent with 3D energy-band calculations. Our data [$\epsilon_2(\omega)$] in the 5–10 eV range are in good agreement with tight-binding calculations of Doni and Parravicini.[14] Further experimental work in p-BN is planned in the 10–40 eV region.

ACKNOWLEDGMENTS

We would like to thank D. A. Lelonis of Union Carbide for providing the pyrolytic boron nitride used in this work. We are grateful to A. W. Moore, Union Carbide for helpful discussions. This work was supported in part by the Department of Energy Grant No. DE-FG05-84ER45151.

[1] J. C. Slonczewski and P. R. Weiss, Phys. Rev. **109**, 272 (1958).
[2] J. W. McClure, *Proceedings of the International Conference on Semimetals and Narrow Gap Semiconductors,* edited by D. L. Carter and R. T. Bate (Pergamon, New York, 1971).
[3] L. G. Johnson and G. Dresselhaus, Phys. Rev. B **7**, 2275 (1973).
[4] A. Zunger, Phys. Rev. B **17**, 626 (1978).
[5] S. Larach and R. E. Shrader, Phys. Rev. **104**, 68 (1956).
[6] J. Cazaux, C. R. Acad. Sci. B **270**, 700 (1970).
[7] R. Vilanove, C. R. Acad. Sci. B **272**, 1066 (1972).
[8] J. Zupan and D. Kolar, J. Phys. C **5**, 3097 (1972).
[9] W. Baronian, Mater. Res. Bull. **7**, 119 (1972).
[10] A. Zunger, A. Katzir, and A. Halperin, Phys. Rev. B **13**, 5560 (1976).
[11] R. Mamy, J. Thomas, G. Jezequel, and J. C. Lemonnier, J. Phys. (Paris) Lett. **42**, 473 (1981).
[12] V. A. Fomichev, Fiz. Tverd. Tela (Leningrad) **13**, 907 (1971) [Sov. Phys.—Solid State **13**, 754 (1971)].
[13] E. Tegeler, N. Kosuch, G. Wiech, and A. Faessler, Phys. Status Solidi B **91**, 223 (1979).
[14] E. Doni and G. P. Parravicini, Nuovo Cimento **64B**, 117 (1969).
[15] M. S. Nakhmanson and V. P. Smirnov, Fiz. Tverd. Tela (Leningrad) **13**, 905 (1971) [Sov. Phys.—Solid State **13**, 752 (1971)]; **13**, 3288 (1971) [**13**, 2763 (1972)].
[16] J. Zupan, Phys. Rev. B **6**, 2477 (1972).
[17] J. Robertson, Phys. Rev. B **29**, 2131 (1984).
[18] R. Taylor and C. A. Coulson, Proc. Phys. Soc. London, Sect. A **65**, 834 (1952).
[19] A. Zunger, J. Phys. C **7**, 76 (1974); **7**, 96 (1974).
[20] R. Dovesi, C. Pisani, and C. Roetti, Int. J. Quantum Chem. **17**, 517 (1980).
[21] A. W. Moore, Nature **221**, 1133 (1969).
[22] R. S. Pease, Acta Crystallogr. **5**, 356 (1952).
[23] R. W. G. Wyckoff, *Crystal Structures* (Interscience, New York, 1948).
[24] R. L. Finicle, Ind. Res. Dev. **25(6)**, 113 (1983).
[25] R. Geick, C. H. Perry, and G. Rupprecht, Phys. Rev. **146**, 543 (1966).
[26] I. L. Babich, Theor. Exp. Chem. (USSR) **8**, 594 (1972).
[27] R. J. Nemanich and S. A. Solin, Bull. Am. Phys. Soc. **29**, 429 (1975).
[28] R. J. Nemanich, S. A. Solin, and R. M. Martin, Phys. Rev. B **23**, 6348 (1981).
[29] T. Kuzuba, K. Era, T. Ishii, and T. Sato, Solid State Commun. **25**, 863 (1978).
[30] T. Kuzuba, Y. Sato, S. Yamaoka, and K. Era, Phys. Rev. B **18**, 4440 (1978).
[31] R. Ramani, K. K. Mani, and R. P. Singh, Phys. Status Solidi B **86**, 759 (1978).
[32] F. Wooten, *Optical Properties of Solids* (Academic, New York, 1972).
[33] F. Wooten, Ref. 32, p. 182.
[34] F. Wooten, Ref. 32, p. 45.